



# On the relevance of molecular diffusion for travel time distributions inferred from different water isotopes

Erwin Zehe<sup>1</sup>, Laurent Pfister<sup>2,3</sup>, Dan Elhanati<sup>4</sup>, Brian Berkowitz<sup>4</sup>

1. Institute of Water and Environment, Karlsruhe Institute of Technology (KIT), 76131 Karlsruhe, Germany

2. Luxembourg Institute of Science and Technology, Environmental Sensing & Modelling Unit, 41 rue du Brill, L-4422 Belvaux, Luxembourg

3. University of Luxembourg, Faculty of Science, Technology and Medicine, 2 place de l'Université, L-4365 Esch-sur-Alzette, Luxembourg

4. Department of Earth and Planetary Sciences, Weizmann Institute of Science, Rehovot 7610001, Israel

Correspondence to: Erwin Zehe ([Erwin.Zehe@kit.edu](mailto:Erwin.Zehe@kit.edu))

**Abstract:** Water isotopes are a tool of choice for assessing travel time distributions of water and chemical species in soils, aquifers and rivers. However, the question of whether different water isotopes tag the same travel time distributions of the water molecule, or whether the inferred travel time distribution is specific to the chosen water isotope, remains under debate. Here we conjecture that the latter is correct. We state that (a) travel time distributions of water and any tracer reflect the spectrum of fluid velocities and diffusive/dispersive mixing between the flow lines connecting the system in- and outlet, and (b) the self-diffusion coefficients of deuterium, tritium and  $^{18}\text{O}$  differ by as much as 10%. Using particle tracking simulations, we show that these differences do indeed affect the variance of the travel time distribution – as one would expect for well-mixed advective-dispersive transport. Moreover, our simulations suggest that in the case of imperfect mixing, also the average travel time becomes sensitive to the differences in self-diffusion coefficients. We find that when advective trapping occurs in low conductive zones, an isotope with a smaller diffusion coefficient remains there for longer times compared to a substance exhibiting faster diffusion. This implies that for imperfectly mixed transport, average transit times ultimately increase with a decreasing self-diffusion coefficient: deuterium has the longest average travel time, followed by tritium, followed by  $^{18}\text{O}$ . Depending on the type of simulated system, we find differences in average travel times ranging from 10 days to more than 2 years. As these differences are in relative terms of order 5-10%, one could be tempted to erroneously explain them as measurement errors. Our findings suggest instead that these differences are physics based. These differences persist and even grow with increasing space and time scales, rather than being averaged out. We thus conclude that travel time distributions inferred from O-H isotopes of the water molecule are conditioned by the chosen water isotope.

## 1 INTRODUCTION

Travel or transit time distributions play a key role in contaminant leaching from the partially saturated zone into groundwater (Sternagel et al., 2021; Klaus et al., 2013; Klaus et al., 2014) and stream flow chemistry in general (Kirchner et al., 2000). As early as 1982, Simmons (1982) and Jury (1982) introduced the concept of travel time and travel distance distributions into soil physics, to acknowledge that field observations of solute transport were frequently inconsistent with predictions of the advection-dispersion model. When injecting a tracer pulse into the soil, the normalized concentration as function of depth characterizes the distribution of travel



46 distances at a fixed time, while the time series of the normalized concentration observed at a  
47 constant depth yields the distribution of times the molecules need to travel to this depth (TTD).  
48 Recalling the theory of linear systems, Simmons (1982) and Jury (1982) advocated the TTD,  
49 also often referred to as solute breakthrough curve (BTC), as the transfer function for simulating  
50 solute breakthrough to a given depth.

51

52 The charm of this approach is that by using alternative transfer functions, one can step beyond  
53 the limitations of advective-dispersive transport. The latter is also called Fickian transport and  
54 reflects the case of perfect mixing, wherein chemical species visit the entire domain and thus  
55 experience the entire spectrum of fluid velocities “many” times. In this case, the central limit  
56 theorem applies, and normally distributed transport distances emerge and the variance in travel  
57 distances grows linearly with time (Roth and Hammel, 1996). Simmons et al. (1982) showed  
58 that a stochastic convective transfer function is well suited to simulate solute transport in the  
59 yet imperfectly mixed near field, where the variance in travel distance grows with the squared  
60 transport time. The general drawback here is that transfer function approaches require linearity  
61 and thus a time invariant velocity field. However, water flow velocities do change nonlinearly  
62 with soil water content, which means that TTD are conditional to (changing) soil water contents  
63 and rainfall forcings. This explains notably why transfer function approaches are (despite their  
64 mathematical appeal) of low practical relevance to predict solute leaching in soils.

65

66 Naturally, the concept of travel time distributions has been generalized to groundwater systems.  
67 Berkowitz and Scher (1995) introduced the continuous time domain random walk to simulate  
68 Fickian and non-Fickian transport of chemical species, which essentially uses transfer functions  
69 characterizing travel time distributions of solutes inferred from observed BTC; see Berkowitz  
70 et al. (2006) for a detailed introduction. A closer look reveals that travel or transit time  
71 distributions can also be defined for entire river basins (McGlynn et al., 2002; McGlynn et al.,  
72 2003; Weiler et al., 2003; Hrachowitz et al., 2009; Hrachowitz et al., 2016; Benettin et al., 2015;  
73 Benettin et al., 2018; Rodriguez et al., 2018; Rodriguez et al., 2021), because catchments or  
74 watersheds drain the collected precipitation to their stream outlet or release it via  
75 evapotranspiration. The defined “inlet” for rainfall and tracers is hence the catchment  
76 surface/soil surface, while the defined outlet is either the riparian zone or the vegetation. As  
77 flow velocities in the stream are several orders of magnitude larger relative to those prevailing  
78 in the subsurface domain, tracer observations at the catchment outlet yield a very good (lumped)



79 approximation of the transit time distribution of water and chemical species through the  
80 catchment system into the stream.

81

82 Early attempts to predict stream flow chemistry relied also on transfer functions and naturally  
83 faced the same problems of state-dependent and seasonally varying travel time distributions  
84 (Hrachowitz et al., 2013; Klaus et al., 2015; Rodriguez et al., 2018). Alternative approaches  
85 rely on age ranked storage in combination with StoreAgeSelection (SAS) functions for, e.g.,  
86 stream flow to infer the respective travel time distributions (Harmann et al. 2015; Rinaldo et  
87 al., 2015). This requires the numerical solution of the Master Equation, i.e., the catchment water  
88 balance for each time and each age (Rodriguez and Klaus, 2019) and an appropriate selection  
89 of the SAS-function, e.g., as a gamma or beta distribution (Hrachowitz et al., 2010; Klaus et  
90 al., 2015; Rodriguez and Klaus, 2019; van der Velde et al., 2012). Recent work reveals that this  
91 approach is even suited to capture fingerprints of preferential flow in the partially saturated  
92 zone (Türk et al, 2025).

93

94 Regardless of whether one favours the transfer function or the SAS approach, water isotopes  
95 are in both cases used as a continuous source of information for transit time distributions at the  
96 pedon (Sprenger et al. 2016) and the catchment scales (McGlynn et al., 2002; McGlynn and  
97 Seibert, 2003; Weiler et al., 2003; Klaus et al., 2013; Sprenger et al., 2016). Yet to date, a  
98 controversial debate prevails as to whether different water isotopes yield information on the  
99 same travel time distribution. Rodriguez et al. (2021) found different median travel times of  
100 deuterium (1.77 y) and tritium (2.19 y) in the 42 ha large Weierbach catchment in Luxembourg.  
101 However, the authors considered these differences as unphysical, because they refer to two  
102 times “the same water molecule” and explained these differences by mere measurement  
103 uncertainty. However, Stewart et al. (2010, 2021) report that average travel times inferred from  
104  $^{18}\text{O}$  and tritium might differ more than one year and argued that these differences are significant  
105 and physics based.

106

107 Here we conjecture that travel time distributions are indeed specific to the chosen water isotope.  
108 More specifically, we argue that (a) TTDs reflect the spectra of fluid velocities along the  
109 flowlines of variable lengths *as well as* diffusive and/or dispersive mixing among them, and (b)  
110 the self-diffusion coefficients of deuterium ( $\text{D}_2\text{O}$  or  $\text{HDO}$ ), tritium ( $\text{HTO}$ ) and  $^{18}\text{O}$  ( $^{18}\text{OH}_2$ )  
111 differ by as much as 10%. At the pore scale, one would thus naturally expect differences, as the



underlying transport process is essentially advective-diffusive. At larger scales, one can observe either Fickian or non-Fickian transport. Fickian transport reflects, as already stated, the asymptotic case of perfect mixing, characterized by normally distributed transport distances in line with the advection-dispersion equation. However, the dispersion coefficient grows with the inverse of the molecular diffusion coefficient, as detailed in section 2.1. Differences in self-diffusion coefficients of water isotopes should hence affect dispersion and thus the variance of travel times. However, one would not expect differences in average travel times, because for advective-dispersive transport the latter is controlled solely by the average fluid velocity. This in turn does not depend on molecular diffusion or on the dispersion coefficient.

Here we conjecture that in the case of imperfect mixing, the average travel time becomes sensitive to differences in diffusion coefficients, as detailed in section 2.1. Anomalous transport can manifest through skewed travel distance distributions leading to a faster first arrival and/or a longer tailing compared to Fickian transport (Levy and Berkowitz, 2003; Edery et al., 2014; Edery et al., 2015; Dentz et al., 2023). Recent experimental work of Elhanati et al. (2025) investigating the breakthrough of deuterium and  $\text{Br}^-$  through saturated columns containing uniform and heterogeneous arrangements of porous media revealed very similar behavior of both tracers, and quantitative analysis demonstrated clearly non-Fickian transport with long tailing of breakthrough curves. Motivated by these findings and the discussion between Stewart et al. (2010, 2021) and Rodriguez et al. (2021), we use physically based numerical simulations to test our conjecture. To this aim, we explore the sensitivity of average travel times to the changes in self-diffusion coefficients, comparing transport of tritium, deuterium and  $^{18}\text{O}$  through media with different types and levels of heterogeneity.

## 2 BACKGROUND AND NUMERICAL SIMULATIONS

### 2.1 Background: Solute transport in porous media in a nutshell

Before detailing the numerical experiments, we briefly revisit the theory of dissolved matter transport, to justify our conceptual and numerical simulation approach. In the simplest case, i.e., dissolved transport of an inert (non-reactive, conservative) substance through a fluid at rest is solely controlled by molecular diffusion. According to Fick's law, the solute flux  $\mathbf{j}$  ( $\text{kg s}^{-1} \text{m}^2$ ) is the product of the molecular diffusion coefficient,  $D_{mol}$  ( $\text{m}^2 \text{s}^{-1}$ ), and the gradient in solute concentration,  $C$  ( $\text{kg m}^{-3}$ ):



144

145

$$\mathbf{j} = -D_{mol} \nabla C \text{ (Eq.1).}$$

146

147 Einstein (1905) showed that molecular diffusion is an effective, macroscopic fingerprint of  
148 Brownian motion. Molecular diffusion ( $D_{mol}$ ) grows with the absolute temperature but  
149 decreases with the viscosity of the fluid and the diameter of the molecule. Moreover, it is well  
150 known that for a fluid at rest and assuming an initial delta distribution of the substance, the  
151 travel distance obeys Gaussian distribution, centered at the origin (Einstein, 1905). The variance  
152 of travel distance grows linearly with time  $t$  (s), while the molecular diffusion coefficient is the  
153 growth factor.

154

155 When the fluid moves with constant and spatially homogeneous velocity,  $\mathbf{v}$  ( $\text{m s}^{-1}$ ), the solute  
156 flux is the sum of an advective and a diffusive component:

157

158

$$\mathbf{j} = \mathbf{v}C - D_{mol} \nabla C \text{ (Eq. 2).}$$

159

160 This is what is meant when loosely stating that the “solute velocity” is not equal to the fluid  
161 velocity. The distribution of travel distances still obeys Gaussian behavior, its variance  
162 increases proportionally to  $D_{mol}$  and  $t$ , while the mean travel distance grows with  $\mathbf{v} t$ . This is  
163 the well-known case of advection-diffusion.

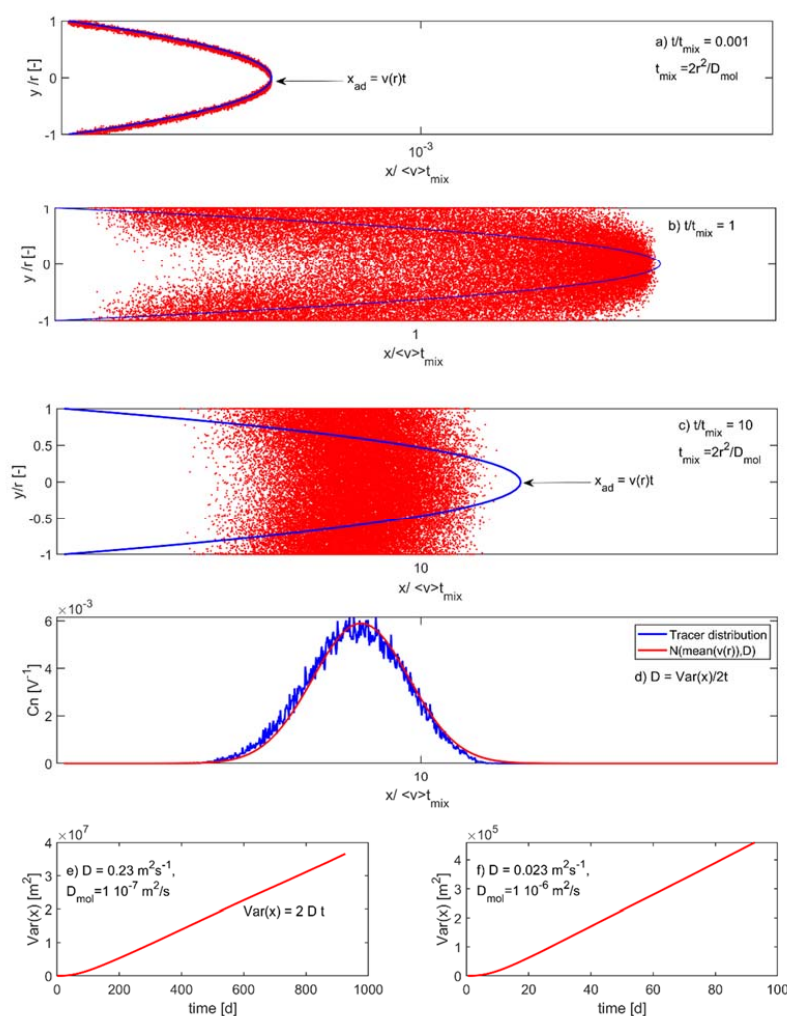
164

165 In line with Einstein’s argument and Roth and Hammel (1996), we note that dispersion is a  
166 macroscopic, effective fingerprint of diffusive mixing of solutes between flowlines of different  
167 fluid velocities. Recalling that water flow in an individual soil pore can be characterized by  
168 Hagen-Poiseuille law, this can be effectively visualized by discussing the migration of a tracer  
169 pulse injected into a pore of radius  $r$  (m) and travelling through the parabolic velocity field. Fig.  
170 1 displays the three main states of Taylor-Aris dispersion, which were all inferred from particle  
171 tracking simulations (see section 2.2) through a parabolic flow field with mean velocity of  $v =$   
172  $10^{-4}$  m/s. For times  $t$  much smaller than the diffusive mixing time scale,  $t_{mix} = \frac{2r^2}{D_{mol}}$ , tracer  
173 molecules migrate along the same flowline and their displacement mirrors essentially the  
174 parabolic flow field (Fig. 1a). In this so-called near field, transport is essentially deterministic  
175 and the variance in travel distance scales with  $t^2$ , as shown in Figs. 1e and 1f for small transport  
176 times. However, the non-uniform displacements in  $x$  directions cause a transversal



177 concentration gradient between the flowlines, which is gradually depleted by transversal  
178 diffusive mixing from fast to slow flowlines and *vice versa* (see Fig. 1b for  $t = t_{mix}$ ). For times  
179 much larger than the diffusive mixing time, all molecules experience the entire velocity field  
180 many times and the central limit theorem applies (Fig. 1 c).

181



182

183 Figure 1: The three stages of Taylor-Aris dispersion in a capillary tube pore with radius  $r$  (m) as a function of the  
184 diffusive mixing time scale  $t_{mix} = 2r^2/D_{mol}$ : (a) near field for  $t \ll t_{mix}$ , intermediate state for  $t = t_{mix}$  (b) and well mixed  
185 far field for  $t \gg t_{mix}$  (c). Variance of particle transport distances as a function of time for  $D_{mol} = 1 \times 10^{-6} \text{ m}^2/\text{s}$  (e)  
186 and  $D_{mol} = 1 \times 10^{-7} \text{ m}^2/\text{s}$  (f). All graphs were inferred from transport simulations based on particle tracking.

187



The comparison of the travel distance distribution inferred from the particles to the Gaussian distribution in Fig. 1c corroborates that indeed a Gaussian travel time distribution eventually emerges. The mean travel distance grows with the spatially averaged fluid velocity,  $\bar{v}$ , and  $t$  (Fig. 1d). The variance of travel times now grows linearly with  $t$  and the slope is the macro-dispersion coefficient  $D$  (Fig. 1e,f). For Taylor-Aris dispersion in a cylindrical pore with radius  $r$ , the dispersion coefficient is determined as:

$$D = \frac{\bar{v}^2 r^2}{D_{mol}} \quad (\text{Eq. 3}).$$

The key point is that  $D$  grows linearly with  $D_{mol}^{-1}$ . Fig. 1 corroborates for the simulated transport of two different tracers with  $D_{mol}$  of  $1 \times 10^{-7}$  (Fig. 1e) and  $1 \times 10^{-6} \text{ m}^2/\text{s}$  (Fig. 1f). Diffusion that is slower by a factor of 10 causes not only a ten times larger dispersion coefficient. It also implies that it takes ten times longer to reach the well-mixed advective-dispersive case and that the variance in travel distances increases ten times faster with time. We can thus state that the macro-dispersion coefficient is an effective, macroscopic fingerprint of subscale diffusive mixing between streamlines of variable of fluid velocities.

Of course, we acknowledge that dispersion in a real-world porous medium relates to the variability in pore sizes and that the geometry and tortuosity of soil pores is clearly more complex than the above example. Yet we argue that Taylor dispersion and Hagen-Poiseuille flow occur in each individual soil pore. This implies the lateral diffusive mixing time for isotopic tracers will be due to their different diffusion coefficients, in each individual soil pore, meaning that the tracer with lower diffusion coefficient will experience a stronger longitudinal dispersion. When a well-defined advective-dispersive transport process emerges, we expect that the variance of travel distances will, hence, still grow with the decreasing molecular diffusion coefficient. However, we do not expect that they will show different mean travel times, simply because advective-dispersion transport relies on a linear superposition of advective and dispersive solute flux, and the average flow velocity  $\bar{v}$  is not affected by changes in the diffusion coefficient.

$$\mathbf{j} = \overset{\text{advective solute flux}}{\bar{v}\bar{C}} - \overset{\text{dispersive solute flux}}{\bar{D}\nabla\bar{C}} \quad (\text{Eq. 4}).$$



220 Instead, we propose that the independence of the average transit time from the diffusion  
221 coefficient no longer holds when non-Fickian transport occurs. The latter breaks the symmetry  
222 of perfect mixing (Bloschl and Zehe, 2005), either because molecules are trapped in low  
223 conductive bottlenecks for very long times, and/or because molecules traveling along rapid  
224 preferential flow paths leave the system after very short times (Berkowitz and Zehe, 2020;  
225 Wienhöfer et al., 2009). As an important implication, the travel time distribution becomes  
226 skewed and in the case of advective trapping in low conductive bottlenecks, one might expect  
227 that an isotope with a smaller diffusion coefficient stays in the bottlenecks for longer times  
228 compared to an isotope which exhibits faster diffusion. This could imply that in case of as for  
229 non-Fickian transport average transit times grow with a decreasing diffusion coefficient.

230

## 231 **2.2 Transport simulations and numerical experiments**

232 To shed light on the role of the different self-diffusion coefficients of deuterium, tritium and  
233 O<sup>18</sup> for the average transit time distributions, we simulated advective-diffusive transport  
234 through steady-state flow fields in 2d saturated domains of increasing heterogeneity, comparing  
235 the transport of the three different water isotopes. The respective self-diffusion coefficients at  
236 a temperature of 25 °C are, according to Devel (1962) and Wang (1952),  $D_{\text{HDO}} = 2.25 \times 10^{-9} \text{ m}^2 \text{ s}^{-1}$ ,  
237  $D_{\text{HTO}} = 2.44 \times 10^{-9} \text{ m}^2 \text{ s}^{-1}$  and  $D_{\text{18OH2}} = 2.66 \times 10^{-9} \text{ m}^2 \text{ s}^{-1}$ . For the case of HTO we  
238 chose to ignore its radioactive decay, to assure that optional differences in average travel times  
239 stem only from the differences in self-diffusion coefficients.

240

241 In all cases we used particle tracking, the particle advancement,  $\Delta s$  (m), being characterized by  
242 the Langevin equation, starting from a given particle location at time  $t_i$ :

243

$$244 \quad \Delta s(x, y) = \mathbf{v}[\mathbf{s}(t_i)]\Delta t + \xi\sqrt{2 D_{mol} \Delta t} \quad (\text{Eq. 5})$$

245

246 The first term characterizes advective displacement, depending on the 2d fluid velocity vector  
247  $\mathbf{v}$ , and the time step  $\Delta t$ . The second term denotes the diffusive displacement, which scales with  
248 a modulus of  $\sqrt{2 D_{mol} \Delta t}$  times a standard normally distributed random number  $\xi$ .

249

250 Three different model scenarios, A, B, and C, are examined, accounting for different types of  
251 hydraulic conductivity fields. Scenario A was inspired by the experimental work of Elhanati et





al. (2025) investigating the breakthrough of deuterium and Br- through homogeneous (uniformly packed) and heterogeneous sand columns (Fig. 2, Scenario A). We simulated steady flow through a 1 m by 10 m block, containing either a sandy or a silty saturated soil, which surrounds a less conductive lens (Fig. 2). The surrounding medium had a hydraulic conductivity of either  $K_s=1\times 10^{-5}$  m/s or  $K_s=1\times 10^{-7}$  m/s and porosity of 0.4 or 0.44, respectively. The low conductive lens had a hydraulic conductivity of either  $K_s=10^{-8}$  m/s or  $K_s=10^{-9}$  m/s. We used a discretization of 0.2 m by 0.2 m, a permeameter type of boundary condition with a head gradient of 0.05 m/m, and calculated the flow field using the model CATLFW (Zehe et al. 2001). We considered no-flow boundary conditions on the horizontal domain boundaries. We simulated advective diffusive transport by using particle tracking according to Eq. 5. As scenario A is an upscaled version of the medium that Elhanati et al. (2025) used in their experiments, we expect that non-Fickian transport will emerge in line with their experimental findings.

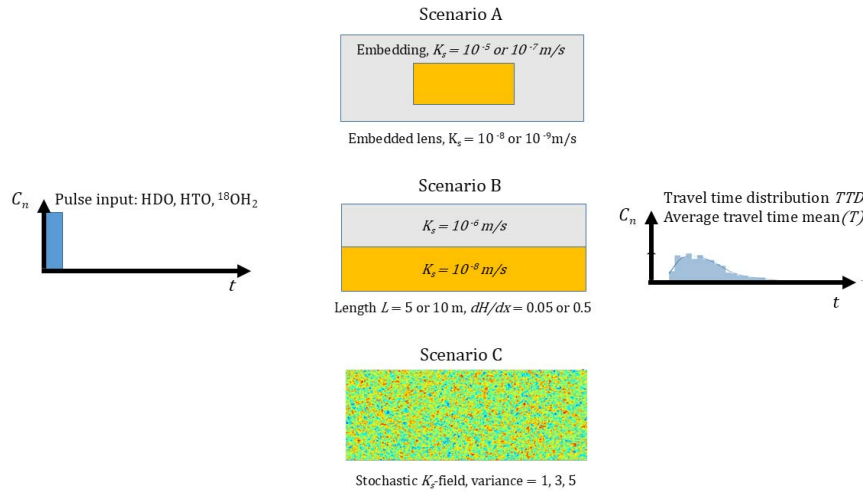


Figure 2: Scheme of model scenarios.

In scenario B, we simulated advective-diffusive solute transport in a simple two-layer aquifer system of 2 m total height and a length of either 5 or 10 m (Fig. 2, Scenario B). The layers with a height of 1m are homogeneous but differ by their saturated hydraulic conductivity  $K_s=10^{-6}$  m/s and  $10^{-8}$  m/s. Both layers were exposed to the same head gradient, which was first set to  $dH/dx = 0.05$  and then to  $dH/dx = 0.5$  to compare two different Peclet numbers. Transport of deuterium, tritium and  $^{18}\text{O}$  with the diffusion coefficients was simulated using a pulse input of



100,000 particles through the left upstream domain, while no-flow conditions were assigned to the two horizontal domain boundaries.

In scenario C (Fig. 2, Scenario C; Fig. 3), we considered steady-state fluid flow within two-dimensional, stochastic heterogeneous media with moderate, intermediate and strong variance in the hydraulic conductivity (Zehe et al., 2021). The 60 m long and 20 m wide domain was discretized into 0.2 m by 0.2 m elements. Flow was driven by a head gradient of  $dH/dx = 1/6$ , from the left upstream boundary to the right downstream boundary, while no-flow conditions were assigned to the two horizontal domain boundaries. We used random and yet statistically homogeneous, isotropic Gaussian fields of three different variance of  $\ln(K)$ , namely 1, 3 and 5 generated with the sequential Gaussian simulator GCOSIM3D (Gómez-Hernández et al., 1997) and a correlation length of 1 m. Advective diffusive transport was again simulated using particle tracking according to Eq. 5. Previous work showed that these media were highly susceptible to preferential flow and transport (Edery et al. 2014; Zehe et al. 2021). We compared simulations for an average hydraulic conductivity of  $K_s = 10^{-7}$  m/s or  $K_s = 10^{-6}$  m/s to account for different Peclet numbers. Fig. 3 shows the hydraulic conductivity fields and the cumulative number of particles that visited a grid cell in the simulation domain for small, medium and large variance for the lower average hydraulic conductivity.

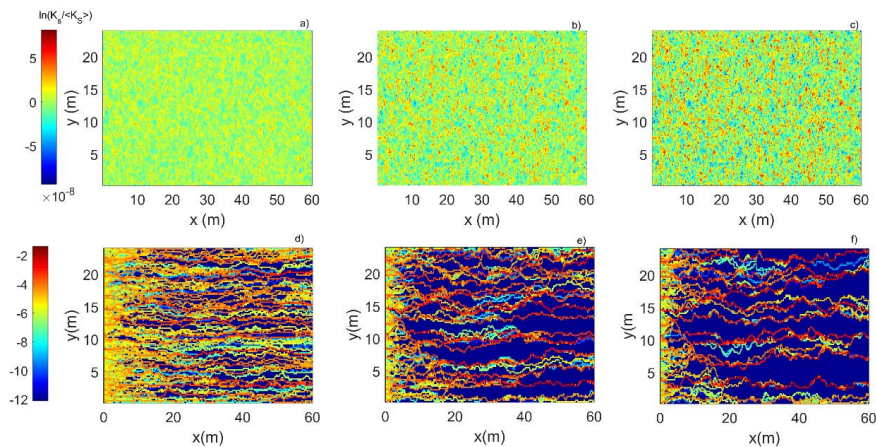


Figure 3: The normalized hydraulic conductivity fields for three randomly selected realizations of small, medium and large variance (a, b, c). Cumulative number of particles ( $N_p$ ) that visited a grid cell in the simulation domain for small, medium and large variance (d, e, f) for HDO.



## 296 3 RESULTS

### 297 3.1 Travel time distributions inferred from scenario A

298 Fig. 4 shows the normalized breakthrough curves of deuterium for the heterogeneous case with  
299 the low conductive embedding, containing either a lower conductive or a higher conductive  
300 clay lens. This reveals, in line with the experimental evidence of Elhanati et al. (2025), a clearly  
301 non-Fickian breakthrough with an earlier first arrival and a significantly longer tailing  
302 compared to the breakthrough curve of the homogeneous system (green dots, Fig. 4). In  
303 addition, Fig. 4 provides average travel times, named  $mean(T)$  hereafter, which correspond to  
304 the first central moment of the normalized breakthrough curve. We find that the average travel  
305 times through the heterogeneous media are, with  $mean(T) = 509.4, 510.3$  and  $515.4$  d, larger  
306 than the average travel time through the homogeneous medium, which is  $mean(T) = 508.4$  d.  
307 Interestingly, we observe that the average travel time declines slightly when the hydraulic  
308 conductivity of the clay lens is increased from  $10^{-9}$  to  $10^{-8}$  m/s. The latter can be explained by  
309 a stronger advective transport of the tracer into the lens, due to the smaller drop in conductivity.  
310 Consistently, we observe an even larger  $mean(T)$  of  $515.4$  d, when elongating the clay lens with  
311  $K_s = 10^{-8}$  m/s by 30%.

312  
313 For convenience, we compared the average travel times,  $mean(T)$ , to the average hydraulic  
314 retention time,  $RT_{hyd}$ , which was calculated by dividing the total pore volume of the domain by  
315 the averaged flow rate.  $RT_{hyd}$  and  $mean(T)$  match, as expected, very well for the case of Fickian  
316 transport through the homogeneous domain. In the case of non-Fickian transport, however, we  
317 observe that the average travel times inferred from the BTCs are slightly larger than suggested  
318 by the hydraulic retention time  $RT_{hyd}$ . This underestimate grows clearly with the length and  
319 thickness of the BTC tails.

320  
321 We generally acknowledge that one can *a priori* expect deviations from Fickian transport in  
322 this setup, as the transport distance is only twice as large as the length of the embedded clay  
323 lens. Yet, the long tail reflects diffusion of molecules into the low conductive lens, which  
324 evidently reside there over considerably long times. The channeling of the flow around the lens  
325 and the enlarged transport velocities explain in turn the earlier arrival of the solutes compared  
326 to the homogeneous case. However, we did not find variations in any of the average travel times  
327 that related to the different self-diffusion coefficients of the isotopic tracers.

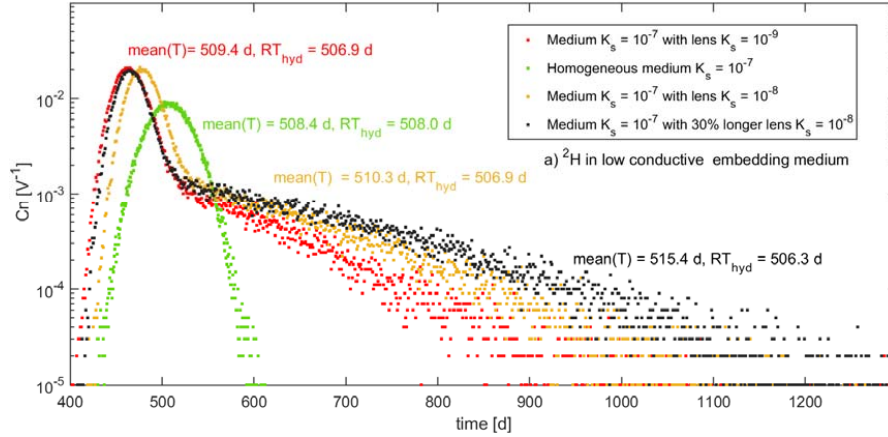


Figure 4: Normalized breakthrough curves of HDO and related average travel times TTD and hydraulic retention times for scenario A for the low conductive embedding medium with  $K_s = 10^{-7} \text{ m s}^{-1}$ .

### 3.2 Travel time distributions inferred from scenario B

Fig. 5 provides the normalized breakthrough curves for case B through the 10 (Fig. 5a, c) and 5 m long layered aquifer (Fig. 5b, d), as a function of the two different head gradients. Average travel times range from the order of 700 d to the short aquifer at the high Peclet (Fig. 5b) to the order of 5300 d for the longer aquifer and the smaller Peclet (Fig. 5c). A closer look reveals that while the breakthrough curves of the three tracers look similar, their corresponding first central moments are indeed different, as shown in the legend of Fig. 5. One can see a clear increase of the average travel time with a declining diffusion coefficient of the isotopic tracers. Deuterium has the smallest self-diffusion coefficient but generally the longest average travel time, while it is *vice versa* for  $^{18}\text{O}$ . For a better comparison we focus on the difference between the average travel time of deuterium and  $^{18}\text{O}$ , defined as:

$$dTT = \text{mean}(T_{\text{HDO}}) - \text{mean}(T_{\text{18OH2}}) \text{ (Eq. 6),}$$

and the relative difference thereof, defined as:

$$dTT_{\text{rel}} = dTT / \text{mean}(T_{\text{18OH2}}) \text{ (Eq. 7).}$$

dTT increases with the length of the system but declines with the Peclet number. Differences in mean travel times, dTT, range from 51 d for the short aquifer and the high Peclet number of



11.1 (Fig. 5b) up to 207 days for the longer aquifer and the small Peclet number of 2.2 (Fig. 5c). Note that the relative differences  $dTT_{rel}$  are small: app. 5% for the small Peclet and they increase to ~10% when increasing the Peclet number.

For both aquifers, we calculated again the hydraulic retention times, using the arithmetic and the geometric means of the hydraulic conductivities of the layers, respectively. The latter was, for the hydraulic gradient of the small Peclet number with  $RT_{hyd} = 1557$  d (4.2 y), more than three times smaller than the average travel times inferred from the tracer breakthrough curves, which was of order 5300 d (Fig. 5c).

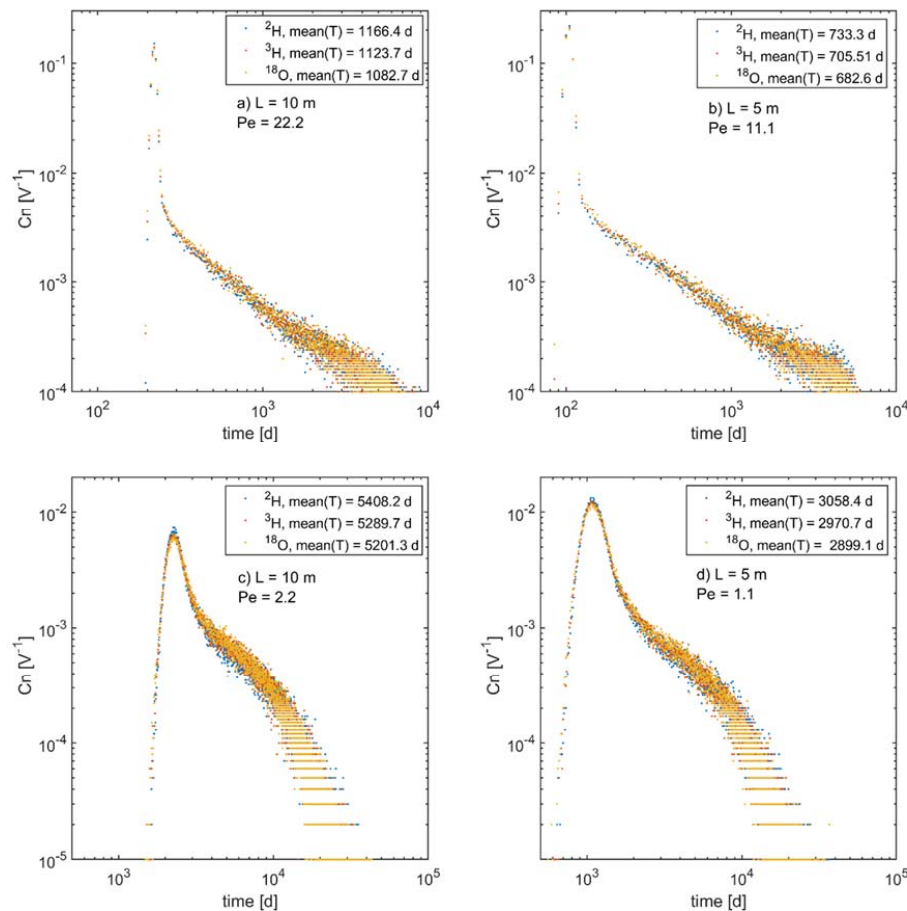


Figure 5: Normalized breakthrough curves of deuterium (<sup>2</sup>H blue dots), tritium (<sup>3</sup>H red dots) and <sup>18</sup>O (yellow dots) and the corresponding average travel times,  $mean(T)$ , for scenario B. Simulations for the 10 m (a, c) and 5 m (b, d) long layered aquifer, for the two head gradients and the corresponding Peclet numbers (Pe). Note that for better visibility panels a and b, as well as c and d, have different scales.



366 The corresponding difference for the shorter aquifer and the high Peclet number is smaller but  
367 still remarkable:  $RT_{hyd}$  is with 578.5 d more than a 100 d smaller than the average travel times  
368 inferred from the particle transport simulations. This underpins that even in the case of simple  
369 layered systems, the analysis of hydraulic retention times may, due to the difference between  
370 fluid and tracer velocities, yield error prone estimates of average tracer travel times.

### 371 **3.3 Travel time distributions inferred from scenario C**

372 Fig. 6 presents the normalized breakthrough and average travel times  $mean(T)$  for scenario C  
373 for all isotopic tracers at transport distances of  $L = 60$  m (a, c, e) and 30 m (b, d, f). The variance  
374 of the hydraulic conductivity field decreases from top to bottom panels, the average  $K_s$  is  $10^{-7}$   
375 m/s. The strength of the “transport anomaly,” i.e., its deviation from Gaussian behavior, clearly  
376 increases with the variance of the hydraulic conductivity field and increasing transport distance.  
377 The larger the variance, the longer the tail of the breakthrough curve. The average travel time  
378 to  $L = 30$  m increases from approximately 1310 days for variance 1, up to approximately 1810  
379 days for variance 5. Note that for  $L = 60$  m the corresponding difference is of the order of 1000  
380 days. Consequently, the average travel time of a tracer for a given transport distance  $L$  increases  
381 strongly with the variance of the hydraulic conductivity field.

382

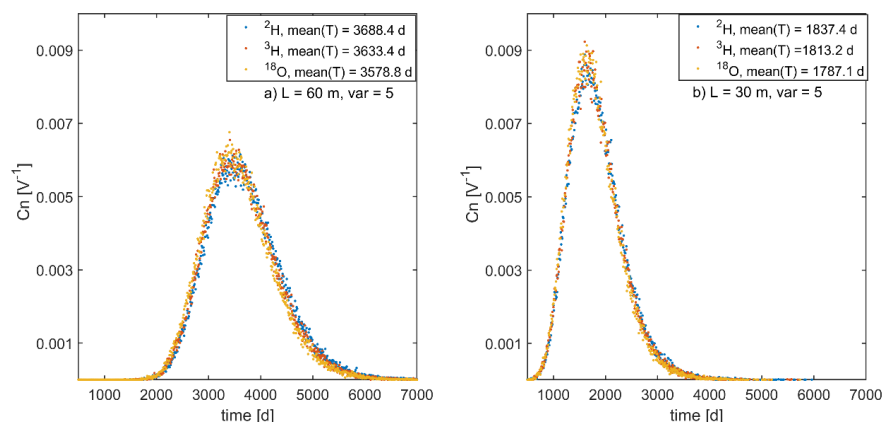
383 Again, we find that the average travel times of the different tracers increase with smaller  
384 diffusion coefficients of the water isotopes. Deuterium has the smallest self-diffusion  
385 coefficient, but in all cases the largest average travel time, due a longer trapping in low  
386 conductive bottlenecks. The related differences between average travel times of deuterium and  
387  $^{18}\text{O}$  rise clearly with increasing variance of the hydraulic conductivity field up to values of a  
388 110 days for the length of 60 m, compared to 50 days for  $L = 30$  m.

389

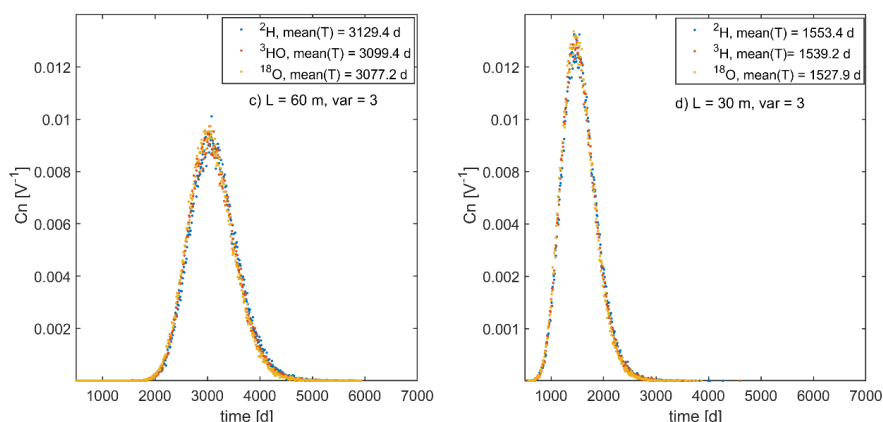
390 However, the average travel times at a given variance grow for each tracer almost  
391 proportionally to the transport distance. This implies that differences in  $mean(T)$  between the  
392 tracers will not average out but grow with increasing transport distance and thus increasing  
393 average travel time. To corroborate this statement, we re-simulated tracer migration through the  
394 conductivity field with the variance 5 while lowering the average  $K_s$  to  $1 \times 10^{-8}$  m/s (Fig. 7).  
395 The differences between the average travel time of deuterium and  $^{18}\text{O}$  are in the order of 2 years  
396 for the long and 1 year for the shorter system.



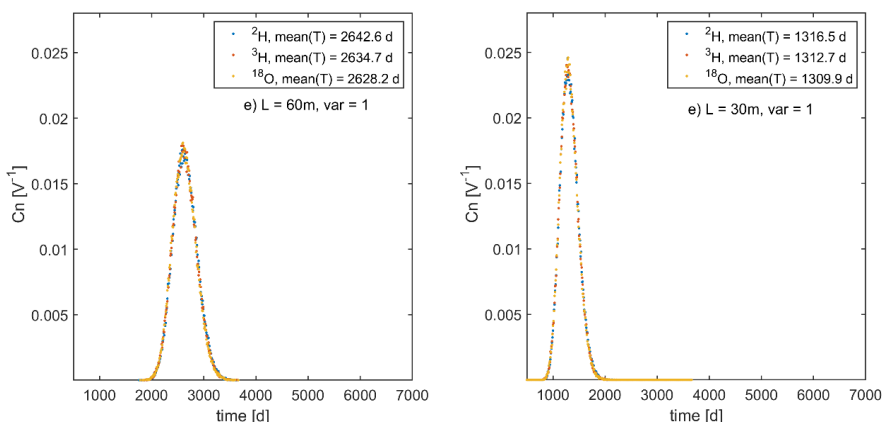
397



398



399



400 Figure 6: Normalized breakthrough and average travel time for scenario C for deuterium ( $^2H$ , blue dots), tritium  
401 ( $^3H$ , red dots) and  $^{18}O$  (yellow dots) and corresponding average travel times  $mean(T)$  after transport distances of  
402 60 m (a, c, e) and 30 m (b, d, f). The variance of the hydraulic conductivity field decreases from top to bottom  
403 panels; the average  $K_s$  is  $10^{-7}$  m/s.  
404





#### 4 DISCUSSION AND CONCLUSIONS

Our study provides clear evidence that the sensitivity of average TTDs to small changes in diffusion coefficients is – albeit relatively small – not a question of measurement error but a question of transport physics. Particularly, for the case of heterogeneous media and anomalous transport we demonstrate that differences in average travel times of different water isotopes (HTO, H<sub>2</sub>O<sup>18</sup>, HDO) can deviate by as much as two years, which corresponds to 3% of the average travel time. We found the strongest relative differences of the order of 10% for a simple two-layered system, consisting of a mobile layer overlying a relatively immobile water storage compartment.

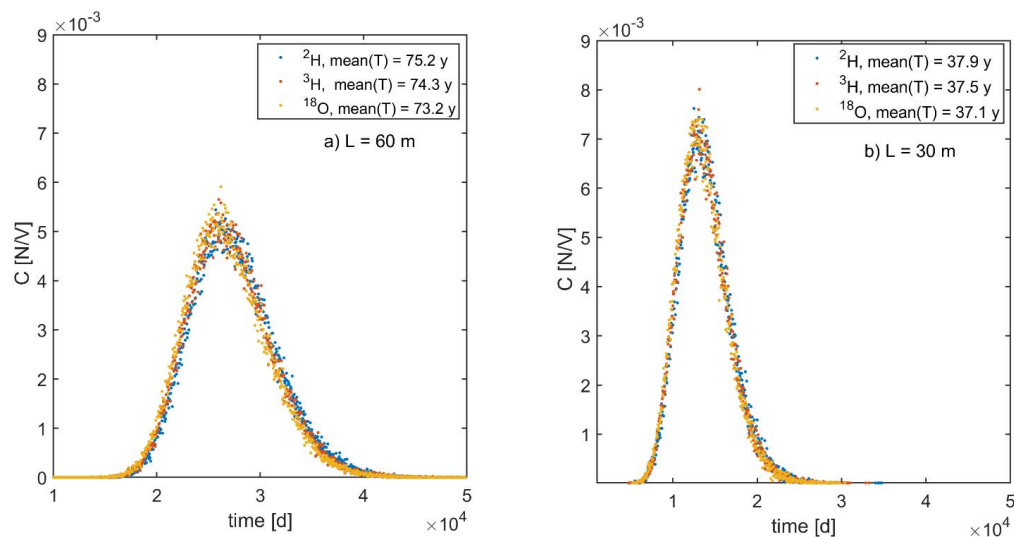


Figure 7: Normalized breakthrough and average travel time for scenario C for deuterium ( $^2\text{H}$ , blue dots), tritium ( $^3\text{H}$ , red dots) and  $^{18}\text{O}$  (yellow dots) and corresponding average travel times  $\text{mean}(T)$  after transport distances of 60 m (a) and 30 m (b). The variance of the hydraulic conductivity field is 5, while the average  $K_s$  is  $10^{-8}$ .

We found smaller differences of the order of 3 to 5% for strongly stochastically heterogeneous media. Given their size, one could be inclined to erroneously interpret these differences as measurement errors. However, these differences are indeed physical and reflect tracers with smaller diffusion coefficients that eventually remain over longer times in low conductive bottlenecks, which enlarges the tails and average travel times. Thus, these effects do not average out, but persist when doubling the transport distances – even despite the total travel distances being 100 times larger than the short correlation length of the hydraulic conductivity field.





427 Our findings are in line with the experiments of Elhanati et al. (2025) and corroborate that water  
428 isotopes show similar behaviors to Br<sup>-</sup>. The molecular diffusion coefficient of bromide is  
429  $2.01 \times 10^{-9} \text{ m}^2/\text{s}$ , indeed close to that of HDO ( $2.22 \times 10^{-9} \text{ m}^2/\text{s}$ ). Our study corroborates  
430 furthermore the argument of Stewart et al. (2010, 2021), namely that averaged travel times  
431 inferred from <sup>18</sup>O might in the case of two-layered mobile and immobile storage regions, or of  
432 a strongly heterogeneous subsurface, be systematically shorter than those inferred from tritium.  
433 The maximum differences we found ranged between 90 d to 1.1 y. The latter corresponds to  
434 the difference Stewart et al. (2010) reported for the Brugga catchment, which has an average  
435 travel time of order 3–6 y for deep groundwater. Stewart et al. (2010) reported an even larger  
436 difference between  $\text{mean}(T_{\text{I8OH2}}) = 3.4 \text{ y}$  to  $\text{mean}(T_{\text{THO}}) = 9.6 \text{ y}$  for the Pukemanga catchment.  
437 We cannot expect to detect similarly large differences here, because we did not account for  
438 radioactive decay of tritium (half-life of 12.32 years). Based on this decay one might detect  
439 contributions of rather old water, that typically cannot be resolved based on differences in <sup>18</sup>O.

440

441 A comparison between the hydraulic retention times, inferred by dividing the storage volume  
442 by the flow, and average travel times, was in accord with the case of well-mixed advective-  
443 diffusive transport. The hydraulic retention times, however, systematically underestimated the  
444 average tracer travel times of the isotopic tracers, when transport was not well-mixed. This  
445 discrepancy can again be explained by diffusive trapping of tracers in rather immobile storage  
446 components: relatively long residence time cause the long tail in the breakthrough curve, which  
447 shifts the average travel time to the right.

448

449 We thus conclude that travel time distributions of isotopic tracers reflect the spectrum of fluid  
450 velocities and diffusive/dispersive mixing between the flow lines connecting inputs and outputs  
451 to the system. Travel time distributions of isotopic tracers might thus reflect the differences in  
452 their diffusion coefficients, which are of order 10%, and in the case of non-Fickian transport  
453 this eventually also affects the mean travel time.

454

455 **Author contributions:** Erwin Zehe conducted most of the analysis and wrote the paper.  
456 Laurent Pfister worked on the part explaining the role of water isotopes for inferring transit  
457 times, provided evidence on their self-diffusion coefficients and contributed to the writing.  
458 Brian Berkowitz contributed to the theory and writing, particularly parts related to non-Fickian  
459 transport and critically overlooked the study.

460

461 **Competing interests.** At least one of the (co-)authors is a member of the editorial board of  
462 Hydrology and Earth System Sciences.



463

464 **Acknowledgements.** B.B. gratefully acknowledges the support of a research grant from the  
465 Israel Science Foundation (Grant No. 1008/20); B.B. holds the Sam Zuckerberg Professorial  
466 Chair in Hydrology. E.Z. B.B. and LP. gratefully acknowledge the support of the ViTamins  
467 project, funded by the Volkswagen Foundation (Grant No. 9B 192/-1), and of the LUNAQUA  
468 project (Grant C21/SR/16167289), funded through the National Research Fund of  
469 Luxembourg. The authors acknowledge support by Deutsche Forschungsgemeinschaft and the  
470 Open Access Publishing Fund of Karlsruhe Institute of Technology (KIT). The service charges  
471 for this open access publication have been covered by a Research Centre of the Helmholtz  
472 Association.

473

## 474 5 REFERENCES

475

- 476 Benettin, P., Rinaldo, A., and Botter, G.: Tracking residence times in hydrological systems:  
477 forward and backward formulations, *Hydrological Processes*, 29, 5203-5213,  
478 10.1002/hyp.10513, 2015.
- 479 Benettin, P., Volkmann, T. H. M., von Freyberg, J., Frentress, J., Penna, D., Dawson, T. E., and  
480 Kirchner, J.: Effects of climatic seasonality on the isotopic composition of evaporating soil  
481 waters, *Hydrology And Earth System Sciences*, 22, 2881-2890, 10.5194/hess-22-2881-2018,  
482 2018.
- 483 Berkowitz, B. & Scher, H., On characterization of anomalous dispersion in porous and fractured  
484 media, *Water Resour. Res.*, **31**(6), 1461–1466, <https://doi.org/10.1029/95WR00483>, 1995.
- 485 Berkowitz, B., Cortis, A., Dentz, M. & Scher, H., Modeling non-Fickian transport in  
486 geological formations as a continuous time random walk, *Reviews of Geophysics*, 44, RG2003,  
487 <https://doi.org/10.1029/2005RG000178>, 2006.
- 488 Berkowitz, B., and Zehe, E.: Surface water and groundwater: unifying conceptualization and  
489 quantification of the two "water worlds", *Hydrology and Earth System Sciences*, 24, 1831-  
490 1858, 10.5194/hess-24-1831-2020, 2020.
- 491 Blöchl, G., and Zehe, E.: Invited commentary - On hydrological predictability, *Hydrological  
492 Processes*, 19, 3923-3929, 2005.
- 493 Dentz, M., Kirchner, J. W., Zehe, E., and Berkowitz, B.: The Role of Anomalous Transport in  
494 Long-Term, Stream Water Chemistry Variability, *Geophysical Research Letters*, 50,  
495 10.1029/2023gl104207, 2023.
- 496 Devel, L.: Measurement of self diffusion in pure water H<sub>2</sub>O-D<sub>2</sub>O mixtures and solutions of  
497 electrolytes. *Acta Chem. Scand.* 16, Vol. 9, 2177 -2188, 1962.
- 498 Edery, Y., Guadagnini, A., Scher, H., and Berkowitz, B.: Origins of anomalous transport in  
499 heterogeneous media: Structural and dynamic controls, *Water Resources Research*, 50, 1490-  
500 1505, 10.1002/2013wr015111, 2014.
- 501 Edery, Y., Dror, I., Scher, H., and Berkowitz, B.: Anomalous reactive transport in porous  
502 media: Experiments and modeling, *Physical Review E*, 91, 10.1103/PhysRevE.91.052130,  
503 2015.



- 504 Einstein, A.: Über die von der molekularkinetischen Theorie der Wärme geforderte Bewegung  
505 von in ruhenden Flüssigkeiten suspendierten Teilchen. *Annalen der Physik*, 17, 549-560, 1905.
- 506 Elhanati, D., Zehe, E., Dror, I., and Berkowitz, B.: Transport behavior displayed by water  
507 isotopes and potential implications for assessment of catchment properties, *EGUsphere*  
508 [preprint], <https://doi.org/10.5194/egusphere-2025-3365>, 2025.
- 509 Hrachowitz, M., Soulsby, C., Tetzlaff, D., Dawson, J. J. C., and Malcolm, I. A.: Regionalization  
510 of transit time estimates in montane catchments by integrating landscape controls, *Water*  
511 *Resources Research*, 45, W05421  
512 10.1029/2008wr007496, 2009.
- 513 Hrachowitz, M., Benettin, P., van Breukelen, B. M., Fovet, O., Howden, N. J. K., Ruiz, L., van  
514 der Velde, Y., and Wade, A. J.: Transit times the link between hydrology and water quality at  
515 the catchment scale, *Wiley Interdisciplinary Reviews-Water*, 3, 629-657, 10.1002/wat2.1155,  
516 2016.
- 517 Jury, W. A., Simulation of solute transport using a transfer function model, *Water Resour.*  
518 *Res.*, **18**(2), 363–368, 1982.
- 519 Klaus, J., Zehe, E., Elsner, M., Kulls, C., and McDonnell, J. J.: Macropore flow of old water  
520 revisited: experimental insights from a tile-drained hillslope, *Hydrology And Earth System*  
521 *Sciences*, 17, 103-118, 10.5194/hess-17-103-2013, 2013.
- 522 Klaus, J., Zehe, E., Elsner, M., Palm, J., Schneider, D., Schroder, B., Steinbeiss, S., van Schaik,  
523 L., and West, S.: Controls of event-based pesticide leaching in natural soils: A systematic study  
524 based on replicated field scale irrigation experiments, *Journal Of Hydrology*, 512, 528-539,  
525 10.1016/j.jhydro1.2014.03.020, 2014.
- 526 Kirchner, J., Feng, X. & Neal, C. Fractal stream chemistry and its implications for contaminant  
527 transport in catchments. *Nature* **403**, 524–527 (2000). <https://doi.org/10.1038/35000537>
- 528 Levy, M., and Berkowitz, B.: Measurement and analysis of non-Fickian dispersion in  
529 heterogeneous porous media, *Journal Of Contaminant Hydrology*, 64, 203-226, 2003.
- 530 McGlynn, B., McDonnell, J., Stewart, M., and Seibert, J.: On the relationships between  
531 catchment scale and streamwater mean residence time, *Hydrological Processes*, 17, 175-181,  
532 2003.
- 533 McGlynn, B. L., McDonnell, J. J., and Brammer, D. D.: A review of the evolving perceptual  
534 model of hillslope flowpaths at the Maimai catchments, New Zealand, *Journal of Hydrology*,  
535 257, 1-26, 2002.
- 536 Rodriguez, N. B., McGuire, K. J., and Klaus, J.: Time-Varying Storage-Water Age  
537 Relationships in a Catchment With a Mediterranean Climate, *Water Resources Research*, 54,  
538 3988-4008, 10.1029/2017wr021964, 2018.
- 539 Rodriguez, N. B., Pfister, L., Zehe, E., and Klaus, J.: A comparison of catchment travel times  
540 and storage deduced from deuterium and tritium tracers using StorAge Selection functions,  
541 *Hydrology and Earth System Sciences*, 25, 401-428, 10.5194/hess-25-401-2021, 2021.
- 542 Sternagel, A., Loritz, R., Klaus, J., Berkowitz, B., and Zehe, E.: Simulation of reactive solute  
543 transport in the critical zone: a Lagrangian model for transient flow and preferential transport,  
544 *Hydrology and Earth System Sciences*, 25, 1483-1508, 10.5194/hess-25-1483-2021, 2021.
- 545 Simmons, C. S., A stochastic-convective transport representation of dispersion in one-  
546 dimensional porous media systems, *Water Resour. Res.*, **18**(4), 1193–1214, 1982.
- 547 Stewart, M. K., Morgenstern, U., and McDonnell, J. J.: Truncation of stream residence time:  
548 how the use of stable isotopes has skewed our concept of streamwater age and origin,  
549 *Hydrological Processes*, 24, 1646-1659, 10.1002/hyp.7576, 2010.
- 550 Stewart, M. K., Morgenstern, U., and Cartwright, I.: Comment on "A comparison of catchment  
551 travel times and storage deduced from deuterium and tritium tracers using StorAge Selection  
552 functions" by Rodriguez et al. (2021), *Hydrology and Earth System Sciences*, 25, 6333-6338,  
553 10.5194/hess-25-6333-2021, 2021.



554 Türk, H., Stumpp, C., Hrachowitz, M., Strauss, P., Blöschl, G., and Stockinger, M.: Catchment  
555 transit time sensitivity to the type of SAS function for unsaturated zone and groundwater,  
556 EGU sphere [preprint], <https://doi.org/10.5194/egusphere-2025-2597>, 2025.  
557 Weiler, M., McGlynn, B. L., McGuire, K. J., and McDonnell, J. J.: How does rainfall become  
558 runoff? A combined tracer and runoff transfer function approach, *Water Resources Research*,  
559 39, 1315  
560 10.1029/2003wr002331, 2003.  
561 Wang, J. H., Robinson, Ch. V., Edelman, I. S.: Measurement of the Self-diffusion of Liquid  
562 Water with, H<sub>3</sub> and O<sub>18</sub> as Tracers. Contribution from the Department of Chemistry of Yale  
563 University, Department of Neurosurgery of New England Center Hospital, and Biophysical  
564 Laboratory of Harvard Medical .School, 1952.  
565 Wienhöfer, J., Germer, K., Lindenmaier, F., Färber, A., and Zehe, E.: Applied tracers for the  
566 observation of subsurface stormflow on the hillslope scale, *Hydrology and Earth System  
567 Sciences*, 13, 2009.  
568 Zehe, E., Loritz, R., Edery, Y., and Berkowitz, B.: Preferential pathways for fluid and solutes  
569 in heterogeneous groundwater systems: self-organization, entropy, work, *Hydrology and Earth  
570 System Sciences*, 25, 5337-5353, 10.5194/hess-25-5337-2021, 2021.  
571  
572